Electronic Transactions on Numerical Analysis.
Volume 11, pp. 94-120, 2000.

ISSN 1068-9613.

ETNA
Kent State University
etna@mcs.kent.edu

NUMERICAL ANALYSIS OF THE RADIOSITY EQUATION USING THE COLLOCATION METHOD*

KENDALL ATKINSON†, DAVID DA-KWUN CHIEN‡, AND JAEHOON SEOL§

Abstract. The collocation method for solving the occluded radiosity equation is examined, theoretically and empirically. Theoretical results are examined, including questions of superconvergence of the collocation solution. The use of "discontinuity meshing" is examined for both piecewise constant and piecewise linear collocation. Also, numerical integration of the collocation integrals is examined, and a near-analytic evaluation method is given.

Key words. radiosity equation, integral equation, numerical integration, collocation methods, discontinuity meshing.

AMS subject classifications. 65R20.

1. Introduction.

The *radiosity equation* is a mathematical model for the brightness of a collection of one or more surfaces when their reflectivity and emissivity are given. The equation is

$$u(P) - \frac{\rho(P)}{\pi}\int_S u(Q)G(P,Q)V(P,Q)\,dS_Q = E(P), \qquad P \in S, \tag{1.1}$$

with $u(P)$ the "brightness" or *radiosity* at P and $E(P)$ the *emissivity* at $P \in S$. The function $\rho(P)$ gives the *reflectivity* at $P \in S$, with $0 \le \rho(P) < 1$. In deriving this equation, the reflectivity at any point $P \in S$ is assumed to be uniform in all directions from P; and in addition, the diffusion of light from all points $P \in S$ is assumed to be uniform in all directions from P. Such a surface is called a *Lambertian diffuse reflector*. The radiosity equation is used in the approximate solution of the 'global illumination problem' of computer graphics; see Cohen and Wallace [10] and Sillion and Puech [21].

The function G is given by

$$\begin{aligned} G(P,Q) &= \frac{\cos\theta_P \cos\theta_Q}{|P-Q|^2} \\ &= \frac{[(Q-P)\cdot\mathbf{n}_P]\,[(P-Q)\cdot\mathbf{n}_Q]}{|P-Q|^4}. \end{aligned} \tag{1.2}$$

In this, $\mathbf{n}_P$ is the inner unit normal to S at P, θ_P is the angle between $\mathbf{n}_P$ and $Q-P$, and $\mathbf{n}_Q$ and θ_Q are defined analogously; cf. Figure 1.1. The function $V(P,Q)$ is a "line of sight" function. More precisely, if the points P and Q can "see each other" along a straight line segment which does not intersect S at any other point, then $V(P,Q) = 1$; and otherwise, $V(P,Q) = 0$. An *unoccluded* surface is one for which $V \equiv 1$ on S, and the numerical solution of this case by some collocation methods was studied previously in [6]. Note that S need not be connected, and it is usually only piecewise smooth. General introductions to the derivation, numerical solution, and application of the radiosity equation (1.1) can be found in the books [10] and [21]. The thesis [17] contains an analysis of the radiosity equation and of the Galerkin method for its solution. In this paper, we consider some practical aspects of the numerical solution of (1.1) by collocation methods when S is occluded.

*Received June 24, 2000. Accepted for publication November 6, 2000. Recommended by D. Calvetti.
†Dept. of Computer Science and Dept. of Mathematics, University of Iowa, Iowa City, IA 52242
‡Dept of Mathematics, California State University - San Marcos, San Marcos, CA 92096
§Program in Applied Mathematical & Computational Sciences, University of Iowa, Iowa City, IA 52242

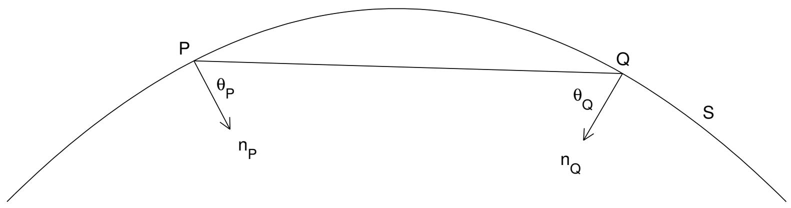

FIG. 1.1. *Illustrative graph for defining radiosity kernel (1.2)*

We often write (1.1) in the simpler form

$$u(P) - \int_S K(P,Q)u(Q)\,dS_Q = E(P), \qquad P \in S, \tag{1.3}$$

or in operator form as

$$(I - \mathcal{K})u = E. \tag{1.4}$$

In §2, we give general stability and convergence results for the collocation solution of this equation. We pay particular attention to the use of piecewise constant and piecewise linear approximants; and we consider the possibility of 'superconvergence' of the approximating solutions. We also give some discussion of the behaviour of the solution.

In §3, we describe our test examples. Two different surfaces are used to illustrate the variety of behaviours which can occur in the radiosity solution; and associated test problems are defined. In addition, experimental calculations are given to illustrate the results given in §2 and to note other phenomena of interest. In §4, we examine the numerical integration of the collocation integrals. There are difficulties in such integrations when the integration element is close to an edge of the surface S. We propose a near-analytic approximation procedure for such integrals. Experimental calculations are given.

2. The Theoretical Framework for Collocation. A number of the results in this report are true for general piecewise smooth surfaces, but we limit our presentation to polyhedral surfaces. The treatment of more general surfaces requires certain nuances which we do not want to consider here; and the problems and methods in which we are interested are illustrated well with polyhedral surfaces. Moreover, many of the surfaces of practical interest are polyhedral.

2.1. The triangulation of S and interpolation over it. Our scheme for the triangulation of S is essentially that described in [3, Chap. 5] and implemented in the boundary element package *BIEPACK,* described in [4]. We subdivide the surface S into closed triangular elements $\{\Delta_j\}$ and we approximate u by a low-degree polynomial over each element. We assume there is a sequence of triangulations of S, $\mathcal{T}_n = \{\Delta_{n,k} \mid 1 \le k \le n\}$, with some increasing sequence of integer values n converging to infinity. In our codes, the values of n

increase by a factor of 4, due to our method for refining a triangulation. To refine a triangle $\Delta_{n,k}$, we connect the midpoints of its sides, creating four new smaller and congruent triangular elements. There are standard assumptions made on the triangulations. We describe the triangulation process briefly, and the details are left to [3, Chap. 5].

Associated with most surfaces are parameterizations of the surface. We assume the surface S can be written as

$$S = S_1 \cup S_2 \cup \cdots \cup S_J,$$

with each S_j a closed polygonal region. Triangulate S_j, say as

$$\{\Delta_{n,k}^j \mid k = 1, ..., n_j\}. \tag{2.1}$$

This need not be a 'conforming triangulation', in contrast to the situation with finite element methods for solving partial differential equations. For S as a whole, define

$$\mathcal{T}_n = \bigcup_{j=1}^{J} \left\{\Delta_{n,k}^j \mid k = 1, ..., n_j\right\}.$$

Often we will dispense with the subscript n in $\Delta_{n,k}^j$, although it is to be understood implicitly. The *mesh size* of this triangulation is defined by

$$h \equiv h_n = \max_{1\le j\le J} \max_{1\le k\le n_j} \text{diameter}(\Delta_{n,k}^j).$$

As noted earlier, the elements of $\mathcal{T}_n$ are denoted collectively by $\mathcal{T}_n = \{\Delta_{n,k} \mid 1 \le k \le n\}$. With each increase of n to $4n$, the mesh h decreases to $\frac{1}{2}h$.

Note that if the mesh is uniform, then

$$n = O\left(h^{-2}\right). \tag{2.2}$$

Although all of our examples use various types of uniform triangulations, one could also consider the use of 'graded meshes' under our schema. In that case, the use of error bounds of the form $O\left(h^p\right)$ would need to be replaced by error bounds of the form $O\left(n^{-q}\right)$.

For functions $f \in L^\infty(S)$ and $k \ge 0$, we write $f \in C^k(S)$ when $f \in C^k(S_j)$ for $1 \le j \le J$. Of course, this implies that f or its derivatives may be discontinous across edges joining adjacent polygonal faces of S. In fact, we often may want to allow this to be true of the reflectivity ρ, the emissivity E, and the radiosity u. Within the context of $L^\infty(S)$, this is not a problem, as such edges form a set of measure zero with respect to the total surface S. Note that this is nonstandard notation, although it serves well our needs in working with the radiosity equation.

For purposes of numerical integration and interpolation over the triangular elements in $\mathcal{T}_n$, we need a parameterization of each such triangular element with respect to a standard reference triangle in the plane, namely the unit simplex

$$\sigma = \{(s,t) : 0 \le s, t, s+t \le 1\}.$$

Let $\Delta_{n,k} \in \mathcal{T}_n$, and let the vertices of $\Delta_{n,k}$ be denoted by $\{v_1, v_2, v_3\}$. Define a parameterization function $m_k : \sigma \underset{onto}{\overset{1-1}{\rightarrow}} \Delta_{n,k}$ by

$$m_k(s,t) = uv_3 + tv_2 + sv_1, \qquad (s,t) \in \sigma, \tag{2.3}$$

ETNA
Kent State University
etna@mcs.kent.edu

with $u = 1 - s - t$. Using this, we can write

$$\int_{\Delta_k} f(Q)\, dS_Q = |D_s m_k \times D_t m_k| \int_\sigma f(m_k(s,t))\, d\sigma, \tag{2.4}$$

since $|D_s m_k \times D_t m_k|$ is a constant function, equal to twice the area of $\Delta_{n,k}$. This formula can be used to numerically evaluate the left-hand integral by using numerical integration formulas developed for the region σ.

The *centroid* of $\Delta_{n,k}$ is defined as

$$P_k = m_k\left(\tfrac{1}{3}, \tfrac{1}{3}\right) = \tfrac{1}{3}\left(v_1 + v_2 + v_3\right). \tag{2.5}$$

Define the operator $\mathcal{P}_n$ associated with piecewise constant interpolation over S by

$$\left(\mathcal{P}_n f\right)(P) = f(P_k), \quad P \in \Delta_k, \quad k = 1, ..., n, \tag{2.6}$$

for $f \in C(S)$. We are not concerned with the values of $\mathcal{P}_n f$ on the boundaries of the elements Δ_k, since $\mathcal{P}_n f$ is to be regarded as an element of $L^\infty(S)$ and needs only to be defined almost everywhere. We want to extend the above definition to all elements of $L^\infty(S)$, and this is described in some detail in [8]. The operator $\mathcal{P}_n$ is a projection on $L^\infty(S)$, and its norm is the same as when it was defined on $C(S)$, namely

$$\|\mathcal{P}_n\| = 1. \tag{2.7}$$

Assuming $f \in C^1(S)$, it is straightforward to show

$$\|u - \mathcal{P}_n u\|_\infty = O\left(h\right). \tag{2.8}$$

We also wish to consider approximations based on piecewise linear approximations over the triangulation $\mathcal{T}_n$. Given $g \in C(S)$, we define the interpolating function $\mathcal{P}_n g$ as follows, basing it on interpolation over the unit simplex σ. Let α be a given constant with $0 \leq \alpha < \frac{1}{3}$; and define interpolation nodes in σ by

$$\{q_1, q_2, q_3\} = \{(\alpha, \alpha), (\alpha, 1 - 2\alpha), (1 - 2\alpha, \alpha)\}. \tag{2.9}$$

If $\alpha = 0$, these are the three vertices of σ; and otherwise, they are symmetrically placed points in the interior of σ. Define corresponding *Lagrange interpolation basis functions* by

$$\ell_1(s,t) = \frac{u - \alpha}{1 - 3\alpha}, \quad \ell_2(s,t) = \frac{t - \alpha}{1 - 3\alpha}, \quad \ell_3(s,t) = \frac{s - \alpha}{1 - 3\alpha},$$

for $(s,t) \in \sigma$ and $u = 1 - s - t$. The linear polynomial interpolating $f \in C(\sigma)$ at the nodes of (2.9) is given by

$$f(s,t) \approx \sum_{i=1}^{3} f(q_i)\ell_i(s,t). \tag{2.10}$$

For $g \in C(S)$, define

$$\left(\mathcal{P}_n g\right)(m_k(s,t)) = \sum_{i=1}^{3} g(m_k(q_i))\ell_i(s,t), \qquad (s,t) \in \sigma, \tag{2.11}$$

ETNA
Kent State University
etna@mcs.kent.edu

for $k = 1, 2, ..., n$. This interpolates $g(P)$ over each triangular element $\Delta_k \subset S$, with the interpolating function linear in the parameterization variables s and t. Let the interpolation nodes in Δ_k be denoted by

$$v_{k,i} = m_k(q_i), \quad i = 1, 2, 3; \quad k = 1, ..., n.$$

Then (2.11) can be written

$$(\mathcal{P}_n g)(P) = \sum_{i=1}^{3} g(v_{k,i})\ell_i(s,t), \qquad P = m_k(s,t) \in \Delta_k, \tag{2.12}$$

for $k = 1, ..., n$. Collectively, we refer to the interpolation nodes $\{v_{k,i}\}$ by $\{v_1, ..., v_{3n}\}$, for $\alpha > 0$.

In the case $\alpha = 0$, the formula (2.11) defines a projection operator on $C(S)$, provided the triangulation is conforming; and easily,

$$\|\mathcal{P}_n\| = 1, \qquad \text{with } \alpha = 0.$$

For $0 < \alpha < \frac{1}{3}$, the function $\mathcal{P}_n g$ is usually not continuous; and if the standard type of collocation error analysis is to be carried out in the context of function spaces, then $C(S)$ must be enlarged to include the piecewise linear approximants $\mathcal{P}_n g$. We do this in exactly the same manner as mentioned above for piecewise constant interpolation over S, done within the context of $L^\infty(S)$. For such α,

$$\|\mathcal{P}_n\| = \frac{1+\alpha}{1-3\alpha}, \qquad 0 < \alpha < \frac{1}{3}. \tag{2.13}$$

A particularly important case is $\alpha = \frac{1}{6}$, for which

$$\|\mathcal{P}_n\| = \frac{7}{3}, \qquad \alpha = \frac{1}{6}. \tag{2.14}$$

Assuming $f \in C^2(S)$, it is relatively straightforward to show

$$\|u - \mathcal{P}_n u\|_\infty = O\left(h^2\right). \tag{2.15}$$

Higher degree piecewise polynomial interpolation can be defined in a manner analogous to the above. In this paper, our numerical examples are restricted to piecewise constant and piecewise linear collocation methods.

2.2. General properties of radiosity equation. The collocation method for solving (1.4) can be written abstractly as

$$(I - \mathcal{P}_n \mathcal{K})u_n = \mathcal{P}_n E, \tag{2.16}$$

with $\mathcal{P}_n$ an interpolatory projection on the function space being used. The first complication arises from the fact that our approximations u_n are generally not continuous over the boundaries of the triangular elements of our mesh for S. Our collocation node points are chosen interior to the elements of the triangular mesh $\mathcal{T}_n$ we impose on S. This is done to avoid having node points on edges of the original surface S, as the normal $\mathbf{n}_P$ in (1.2) is undefined where two edges come together. For our function space setting for (1.4) and (2.16), we use the Banach space $\mathcal{X} = L^\infty(S)$, as discussed earlier.

ETNA
Kent State University
etna@mcs.kent.edu

There are two possible approaches to the analysis of collocation methods for solving (1.1) or (1.4). The first approach combines the result

$$\|\mathcal{K}\| < 1 \tag{2.17}$$

and the geometric series theorem. The second approach uses the observation that when considered locally to the edge common to two faces of subsurfaces of S, the operator $\mathcal{K}$ is a 'Mellin convolution integral operator'. We discuss both approaches in this section, emphasizing the former.

For the origins of (2.17), we note the following result proven in [6].

LEMMA 2.1. *Assume Γ is the boundary of a bounded convex open set $\Omega \subset \mathbb{R}^3$, and assume Γ is a surface to which the Divergence Theorem can be applied. Let $P \in \Gamma$, and let Γ be smooth in an open neighborhood of P. Then $G(P,Q) \geq 0$ for $Q \in \Gamma$, and*

$$\int_{\Gamma} G(P,Q)\, d\Gamma_Q = \pi. \tag{2.18}$$

With this theorem, we can obtain the result

$$\int_{S} G(P,Q)V(P,Q)\, dS_Q \leq \pi \tag{2.19}$$

at each point $P \in S$ for which S is smooth in some neighborhood of P. Since we assume that S is polyhedral, this means for all points P in the interior of the polygonal faces of S. The proof is similar, although slightly more complicated, to that given in [5]; and we omit it here. Using (2.19) and the definition of $\mathcal{K}$, we have

$$\frac{\rho(P)}{\pi} \int_{S} G(P,Q)V(P,Q)\, dS_Q \leq \rho(P) \leq \|\rho\|_\infty\,,$$

for all points $P \in S$ except for those belonging to an edge of one of the polygonal faces of S (a set of measure zero). From this, we have

$$\|\mathcal{K}\| \leq \|\rho\|_\infty\,.$$

We assume that $\|\rho\|_\infty < 1$, and thus (2.17) follows for $\mathcal{K}$ as an operator on $L^\infty(S)$ to $L^\infty(S)$.

2.3. A convergence theory based on the geometric series theorem. The principal means of analyzing numerical schemes for solving the radiosity equation has been to base the stability analysis on the geometric series theorem. With (2.17), it clearly follows that $(I-\mathcal{K})^{-1}$ exists as a bounded linear operator from $L^\infty(S)$ to $L^\infty(S)$, and

$$\left\|(I-\mathcal{K})^{-1}\right\| \leq \frac{1}{1-\|\mathcal{K}\|}.$$

For the stability analysis of (2.16), begin with

$$\|\mathcal{P}_n\mathcal{K}\| \leq \|\mathcal{P}_n\|\, \|\mathcal{K}\|\,. \tag{2.20}$$

If we have

$$B \equiv \left[\sup_n \|\mathcal{P}_n\|\right] \|\mathcal{K}\| < 1, \tag{2.21}$$

ETNA
Kent State University
etna@mcs.kent.edu

then we have $(I - \mathcal{P}_n\mathcal{K})^{-1}$ exists as a bounded operator on $L^\infty(S)$, for all $n \geq 1$. Moreover,

$$\left\|(I - \mathcal{P}_n\mathcal{K})^{-1}\right\| \leq \frac{1}{1-B}. \tag{2.22}$$

For the comparison of the solutions u and u_n, the respective solutions of (1.4) and (2.16), it is straightforward to obtain

$$u - u_n = (I - \mathcal{P}_n\mathcal{K})^{-1}(u - \mathcal{P}_n u). \tag{2.23}$$

This leads to the bounds

$$\frac{\|u - \mathcal{P}_n u\|}{1+B} \leq \|u - u_n\|_\infty \leq \frac{\|u - \mathcal{P}_n u\|}{1-B}, \qquad n \geq 1. \tag{2.24}$$

The speed of uniform convergence of u_n to u is exactly that of $\mathcal{P}_n u$ to u. Thus the regularity of u will affect the rate of convergence of u_n, a point we discuss further below. The bound (2.24) is not the entire story, as it is sometimes possible to obtain more rapid convergence at selected points, a phenomena known as 'superconvergence'. We discuss this in the context of particular methods.

2.4. The centroid method. When $\mathcal{P}_n$ is the piecewise constant interpolatory projection of (2.6), we refer to the collocation method as the *centroid method*. With it, we have $\|\mathcal{P}_n\| = 1$; and when combined with (2.17), we have (2.21) with $B < 1$. Thus the centroid method is stable and convergent. What is its speed of convergence? This depends on a number of factors, including the nature of the surface S, the regularity of the solution u, and the way in which the triangulation $\mathcal{T}_n$ has been defined. From (2.8), we have that if $u \in C^1(S)$, then (2.24) implies

$$\|u - u_n\|_\infty = O(h) \equiv O\left(n^{-1/2}\right). \tag{2.25}$$

We now discuss various extensions of this result.

Suppose that the closed polyhedral faces S_j of S are disjoint. Then we can show that if $u \in C^2(S)$, then

$$\max_{1 \leq i \leq n} |u(P_i) - u_n(P_i)| = O(h^2) \equiv O\left(n^{-1}\right), \tag{2.26}$$

with $\{P_i\}$ the centroids of the triangulation $\mathcal{T}_n$.

To begin, we introduce the iterated collocation solution

$$\widehat{u}_n = E + \mathcal{K}u_n.$$

It follows that

$$\begin{aligned} \mathcal{P}_n\widehat{u}_n &= u_n, \\ (I - \mathcal{K}\mathcal{P}_n)\,\widehat{u}_n &= E. \end{aligned} \tag{2.27}$$

The solvability of (2.27) is equivalent to that of the original collocation method (2.16), and

$$(I - \mathcal{K}\mathcal{P}_n)^{-1} = I + \mathcal{K}(I - \mathcal{P}_n\mathcal{K})^{-1}\mathcal{P}_n.$$

With (2.27), we have

$$u - \widehat{u}_n = (I - \mathcal{K}\mathcal{P}_n)^{-1}\mathcal{K}(I - \mathcal{P}_n)\,u, \tag{2.28}$$

ETNA
Kent State University
etna@mcs.kent.edu

and it is then possible to prove

$$\max_j |u(P_j) - u_n(P_j)| \leq c \max_j |\mathcal{K}(I - \mathcal{P}_n)\, u(P_j)|\,, \tag{2.29}$$

with $\{P_j\}$ the collocation nodes used in defining $\mathcal{P}_n$. For a complete development of iterated projection methods, see [3, p. 71]. For a proof of (2.29), see the derivation given in [3, pp. 449-450]. These results are valid for all piecewise polynomial collocation methods for solving the radiosity equation, not just the centroid method.

Returning to the proof of (2.26), assume that the closed polyhedral faces S_j of S are disjoint and that $u \in C^2(S)$. Then it is straightforward to show that

$$\|\mathcal{K}(I - \mathcal{P}_n)\, u\|_\infty = O\left(h^2\right),$$

thus showing (2.26). For a closely related derivation, see [3, p. 81]. The proof depends crucially on the fact that over each triangular face Δ_k,

$$\int_{\Delta_k} u(Q)\, dS_Q = \text{area}\left(\Delta_k\right)\, u\left(P_c\right)$$

if $u(P)$ is a linear polynomial and P_c is the centroid of Δ_k.

2.4.1. Singular behaviour. If the surface S has polygonal faces which join along an edge L, then it is generally not possible to improve upon (2.25):

$$\max_{1 \leq i \leq n} |u(P_i) - u_n(P_i)| = O(h) \equiv O\left(n^{-1/2}\right), \tag{2.30}$$

for $u \in C^2\left(S\right)$. This is the same as $\|u - u_n\|_\infty$ from (2.25), and it is primarily because of the error behaviour adjacent to the edge L. A sketch of a proof is given in [6, p. 281], although it was for piecewise linear collocation rather than the centroid method.

More importantly, along such edges L, we can have algebraic singularities in the solution u. For simplicity, assume the edge L is a subinterval of the x-axis in $\mathbb{R}^3$, and assume that one of the polygonal faces containing L is contained in the xy-plane, $y > 0$. Then within this plane, the solution u is likely to have the behaviour

$$u(x, y, 0) = O\left(y^\alpha\right), \qquad y \to 0, \tag{2.31}$$

with $0 < \alpha < 1$; and an analogous situation holds in the other face bordering L. A detailed derivation of this behaviour is given in Rathsfeld [16, Thm. 1.2]. The exponent α varies with both the angle in the surface S at the edge L and the reflectivity ρ on the faces bordering L.

For functions satisfying (2.31), it is relatively straightforward to show that

$$\|u - \mathcal{P}_n u\|_\infty = O\left(h^\alpha\right). \tag{2.32}$$

In analogy with the results in [9] for one-dimensional Mellin convolution integral equations, and using the results in [16], we expect that one can improve the rate of convergence to $O(n^{-1/2})$, or even $O(n^{-1})$ at the centroids of $\mathcal{T}_n$, provided a suitably graded mesh is used in creating the triangulation $\mathcal{T}_n$. We do not consider this further in this paper, preferring to study how the behaviour of the solution affects the rate of convergence of u_n to u when a 'uniform' triangulation scheme is used.

2.4.2. Using a discontinuity meshing. One of the effects of occlusion is to produce 'shadows' on portions of the surface S. For the planar radiosity equation, the effects of these shadows on the differentiability are studied in [5]. The situation in $\mathbb{R}^3$ can be considerably more complicated. Our test surfaces S, shown in Figures 3.1 and 3.2, have the edges of subsurfaces all parallel to the coordinates axes, a highly artificial situation. The case with more general polyhedral surfaces is studied in Seol [20]. Nonetheless, most of our discussion for numerical schemes in the presence of such shadow lines will transfer to the more general situation.

What has been recommended in the literature is to use a 'discontinuity meshing' scheme, not allowing the shadow lines to intersect with the interiors of the elements of the triangulation. An example of such is given in Figure 3.3 for the surfaces in Figures 3.1 and 3.2. There are two possible reasons for wanting to use such a meshing scheme; and in some cases, such a discontinuity meshing is actually not needed, at least as it affects the order of convergence of the collocation scheme.

Assuming that the unknown radiosity u has a discontinuous derivative along the shadow line, usually perpendicular to that line, this can affect the order of convergence of $\|u - \mathcal{P}_n u\|_\infty$, and thus also that of $\|u - u_n\|_\infty$. There are two cases of interest, and they are most easily studied and illustrated for functions of one variable.

Consider a function f defined on $[0, 1]$ and assume we have the mesh

$$t_j = \frac{j}{n}, \qquad j = 0, 1, \ldots, n. \tag{2.33}$$

Approximate f with piecewise constant functions, interpolating f at the midpoint of each subinterval $[t_{j-1}, t_j]$, $j = 1, \ldots, n$.

For the first case, assume f has a bounded discontinuity in f' at $t = \zeta \in (0, 1)$, generally with ζ not a mesh point. Then it is straightforward to show the following.

SF Assume $f'(t)$ is continuous on $[0, \zeta]$ with a finite limit $f'(\zeta - 0)$; and similarly, assume $f'(t)$ is continuous on $[\zeta, 1]$ with a finite limit $f'(\zeta + 0)$. Then the piecewise constant interpolating function $f_n(t)$ satisfies

$$\|f - f_n\|_\infty = O(h). \tag{2.34}$$

In addition, if $g \in C^1[0, 1]$ and if f'' is twice-continuously differentiable on $[0, \zeta]$ and $[\zeta, 1]$, then

$$\int_0^1 g(t)\,[f(t) - f_n(t)]\, dt = O\left(h^2\right). \tag{2.35}$$

This implies that no discontinuity meshing is needed in this case, either to obtain the correct order of uniform convergence in the collocation scheme or to obtain superconvergence at the midpoints of the mesh.

These results extend to the two-dimensional case in a straightforward way. The generalization of (2.35) is the tool used to show the right side of (2.29) is $O(h^2)$. Assuming that u can be extended to a twice-continuously differentiable function on the closure of the region on each side of the shadow line, it follows that the order of convergence results are unaffected by whether or not a discontinuity meshing is used. This is illustrated in the following section in Figure 3.5, although the accuracy is greater when using a discontinuity meshing. As a note of caution, these results do not extend to the piecewise linear collocation method, which we discuss and illustrate below.

For the second case of interest, assume the function $f'(t)$ has an unbounded derivative at ζ. Then the order of convergence results are affected. Assume that

$$f(t) = \begin{cases} f(\zeta) + (\zeta - t)^{\alpha} k_1(t), & 0 \le t < \zeta, \\ f(\zeta) + (t - \zeta)^{\alpha} k_2(t), & \zeta < t \le 1, \end{cases} \tag{2.36}$$

with $0 < \alpha < 1$, $k_1 \in C^2[0, \zeta]$, and $k_2 \in C^2[\zeta, 1]$. It is straightforward and well-known that

$$\|f - f_n\|_\infty = O\left(h^{\alpha}\right), \tag{2.37}$$

and

$$\int_0^1 g(t)\left[f(t) - f_n(t)\right] dt = O\left(h^{1+\alpha}\right). \tag{2.38}$$

To recapture the optimal order of convergence, given in (2.34)-(2.35), it is necessary to use a graded mesh in a neighborhood of the singular point ζ. The construction of this graded mesh is explored in depth in [3, Section 4.2.5], and we omit it here. Again, these results extend to the two-dimensional case, and such graded meshes are explored in Rathsfeld [16]. Usually, however, the type of behaviour seen in (2.36) is not seen along shadow lines, but rather along the common edge of two subsurfaces of S, as discussed above following (2.31). The graded mesh is still needed to restore an optimal order of convergence, but the discontinuity mesh would not be needed in such a case, at least as it affects the order of convergence.

2.5. Piecewise linear collocation. Recall the piecewise linear interpolatory function of (2.12) with the interpolation parameter $\alpha \in (0, 1)$. There are three collocation node points within each triangular element, and thus there are $3n$ node points on the surface S. To carry out the stability analysis of Subsection 2.3, we need to require

$$\|\rho\|_\infty \frac{1+\alpha}{1-3\alpha} < 1.$$

For the important case of $\alpha = \frac{1}{6}$, this means requiring

$$\|\rho\|_\infty < \frac{3}{7}, \tag{2.39}$$

which is a fairly stringent restriction. For surfaces S without subsurfaces joining at some common edge (e.g. the surface in Figure 3.1), the operator $\mathcal{K}$ is compact on $L^\infty(S)$. This means we can use a standard analysis (cf. [3, Chap. 3]) to justify the piecewise linear collocation method, obtaining again the error bound (2.24). But with some subsurfaces of S joining at a common edge (e.g. the surface in Figure 3.2), $\mathcal{K}$ is no longer compact and another type of stability and error analysis must be used. For cases such as that in in Figure 3.2, the analysis of [16] can be used to give the needed stability analysis. But if the surface contains a vertex that is interior to S, then no means of analysis is known at present.

2.6. Rates of convergence. We now consider the rates of convergence to be expected in the situations discussed earlier for the centroid method. We assume that the piecewise linear collocation method is stable,

$$\left\|\left(I - \mathcal{P}_n\mathcal{K}\right)^{-1}\right\| \le c < \infty, \qquad n \ge N, \tag{2.40}$$

for some N. If the radiosity solution $u \in C^2(S)$, then it is straightforward to show

$$\|u - \mathcal{P}_n u\|_\infty = O\left(h^2\right),$$

and therefore,

$$u - u_n = O\left(h^2\right). \tag{2.41}$$

If the surface S is composed of disjoint subsurfaces S_j, then we can obtain superconvergence results at the collocation node points. In particular, if we use $\alpha = \frac{1}{6}$, then

$$\max_{1 \le i \le 3n} |u(P_i) - u_n(P_i)| = O\left(h^4\right). \tag{2.42}$$

This reduces to $O\left(h^3\right)$ in the case of other $\alpha \in \left(0, \frac{1}{3}\right)$. A proof is given in [6].

As with the centroid method, if S contains polygonal faces which join along an edge L, then the result (2.41) is the best that can be expected, for all choices of $\alpha \in \left(0, \frac{1}{3}\right)$. This is discussed in [6, pp. 281-282]. Moreover, the presence of singular behaviour such as (2.31) leads to the rate of convergence shown in (2.32). Again, a suitably graded mesh is needed in order to restore the order of convergence given in (2.41)-(2.42). This is also true if the singular behaviour occurs along some other line in S, perhaps a shadow line, rather than just at an edge of S. These results are illustrated in Section 3.

2.6.1. Using a discontinuity meshing. Consider the earlier single-variable example given following (2.33). For piecewise linear interpolation, use the interpolation node points

$$\begin{aligned} t_{j,1} &= \frac{1}{2}\left(t_{j-1} + t_j\right) - \beta\left(t_j - t_{j-1}\right), \\ t_{j,1} &= \frac{1}{2}\left(t_{j-1} + t_j\right) + \beta\left(t_j - t_{j-1}\right), \end{aligned}$$

for some $\beta \in \left(0, \frac{1}{2}\right)$, $1 \le j \le n$. An optimal special choice is $\beta = \frac{\sqrt{3}}{2}$, leading to the Gauss-Legendre zeros of order 2 relative to $[t_{j-1}, t_j]$. For the above case in Subsection 2.4.2 of **SF** for the centroid method, and with any such $\beta \in \left(0, \frac{1}{2}\right)$, the results (2.34)-(2.35) are still valid; and more importantly, they cannot be improved.

As before, these results extend to the case of triangulations $\mathcal{T}_n$ over S. Thus, a discontinuity meshing is needed in order to recover the convergence results of (2.41)-(2.42). This is illustrated in Figure 3.7 of the following Section 3.

2.7. The linear system. Let the number of collocation nodes be denoted by d_n ($d_n = n$ for the centroid method, $d_n = 3n$ for the piecewise linear method), and let $\{P_i\}$ denote collectively these nodes. Let $\{\varphi_i \mid i = 1, \ldots, d_n\}$ denote the Lagrange basis functions for the interpolation scheme being used. For the centroid rule,

$$\varphi_i(P) = \begin{cases} 1, & P \in \Delta_i, \\ 0, & P \notin \Delta_i. \end{cases}$$

For piecewise linear interpolation, use the basis functions implicit in (2.12), which are again nonzero over only a single triangular element. We also will write

$$\varphi_{k_{j,\ell}}(Q), \qquad k_{j,\ell} = 3j - 3 + \ell, \quad \ell = 1, 2, 3,$$

for the three linear basis functions over the element Δ_j. Also introduce the parameter $\nu = 1$ for the centroid method, and $\nu = 3$ for the piecewise linear method.

The solution of (2.16), namely $(I - \mathcal{P}_n\mathcal{K})u_n = \mathcal{P}_n E$, reduces to the solution of the linear system

$$u_n(P_i) - \sum_{j=1}^{n}\sum_{\ell=1}^{\nu} u_n(P_{k_{j,\ell}}) \int_{\Delta_j} V(P_i, Q) G(P_i, Q) \varphi_{k_{j,\ell}}(Q)\, dS_Q = E(P_i), \tag{2.43}$$

with $\left\{P_{k_{j,\ell}} : 1 \le \ell \le \nu\right\}$ the ν collocation nodes inside Δ_j, for $i = 1, \ldots, d_n$. In practical problems, d_n can be quite large, namely 10,000 or larger. For larger values of d_n, it is impractical to setup this system completely, and so-called "fast matrix-vector multiplication methods" are needed. An example of such is given in [7] for unoccluded surfaces, and other schemes have been given, based on the "fast multipole method" and wavelet compression multi-resolution schemes.

In setting up this system, simplifications are possible. First, if P_i and Δ_j are contained in the same polyhedral face of S, then $G(P_i, Q) \equiv 0$. Second if a viewer at P_i cannot see any portion of Δ_j, then the corresponding integral is zero. Thus it is important to create view information of this kind for all of the elements of $\mathcal{T}_n$ and all the collocation nodes P_i.

An important consideration is knowing how to calculate the integrals in (2.43) for which only a portion of Δ_j can be seen from P_i. In a number of cases, these integrals have been estimated by various crude schemes, in the interest of speeding the setup of the linear system. All of these schemes have an error of size $O(h)$ in their impact on the accuracy of u_n. Thus all superconvergence phenomena are destroyed; and the higher rate of convergence associated with piecewise linear interpolation is also destroyed. These integrals, in which only a portion of Δ_j can be seen from P_i, must be calculated as accurately as the remaining integrals in the linear system. Determining the portion of Δ_j which can be seen from P_i is, however, quite a difficult task, and we do not attempt any kind of general solution here.

In Section 4 we give a direct way to evaluate all of the integrals in (2.43) for the centroid method, and we give a very fast way to evaluate them for piecewise linear interpolation. Without sufficiently accurate evaluation of these integrals, the faster rates associated with superconvergence and piecewise linear interpolation are destroyed.

3. Numerical Examples. Dealing with the general case of occluded polyhedral surfaces was too daunting a task, as it requires a fairly sophisticated framework to handle the subsurfaces of S, along with being able to determine the occluded regions as the field point varies. Moreover, it was not necessary for our experimental study of the effects of various types of surface behaviour and solution behaviour. We have used two surfaces for our experiments. We believe that these two surfaces, together with suitably chosen test cases u, are sufficient to examine experimentally a number of properties of the numerical analysis of the occluded radiosity equation.

3.1. The experimental surfaces.

- The 4-piece surface. The surface consists of four square subsections, denoted by S_1, S_2, S_3, S_4.
  - $S_1 = [0, A] \times [0, A]$ in the xy-plane;
  - S_2 and S_3 are the bottom and top, respectively, of $[0, B] \times [0, B]$ in the plane $z = 1$;
  - $S_4 = [0, C] \times [0, C]$ in the plane $z = 2$.

  This surface S is illustrated in Figure 3.1. We choose the parameters A, B, C to satisfy

  $$C < B, \qquad 2B < A. \tag{3.1}$$

  The surface has shadow lines in S_1 along the boundaries of the squares $[0, 2B - C] \times [0, 2B - C]$ and $[0, 2B] \times [0, 2B]$.
- The 5-piece surface. This surface S consists of the 4-piece surface together with the additional face S_5:

$$S_5 = \{(x, A, z) : 0 \le x \le A,\ 0 \le z \le 1\}.$$

ETNA
Kent State University
etna@mcs.kent.edu

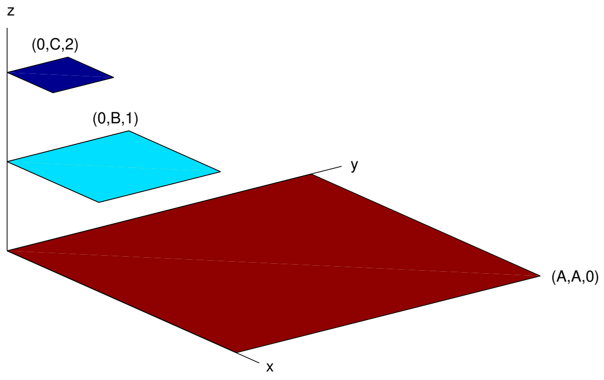

FIG. 3.1. *The 4-piece surface*

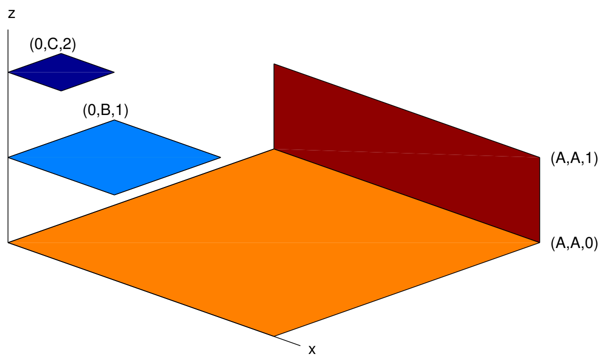

FIG. 3.2. *The 5-piece surface*

Thus the surface has an edge, where S_1 and S_5 are in contact. This surface S is illustrated in Figure 3.2, and the parameters A, B, C satisfy the same restrictions as for the 4-piece surface.

A surprising number of phenomena can be studied with the use of only these two quite simple surfaces. In all of our examples, we use $(A, B, C) = (5, 2, 1)$.

We have shadow lines in S_1, and these can be used to study the effect of triangulating S_1 in various ways. For our first type of triangulation scheme, we define the initial triangulation of S_1 by breaking it into two triangular elements, dividing S_1 by using the diagonal line from $(0, 0, 0)$ to $(A, A, 0)$; and an analogous initialization is used with the remaining rectangles S_2, S_3, S_4, S_5. The subsequent triangulations $\mathcal{T}_n$ are derived by applying the standard re-

ETNA
Kent State University
etna@mcs.kent.edu

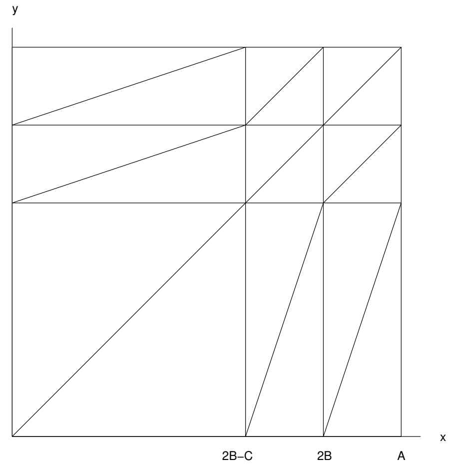

FIG. 3.3. *The initial discontinuity mesh for subsurface* S_1

finement procedure to this initial triangulation. We refer to this triangulation as our *uniform mesh*. The second triangulation procedure is to respect the shadow lines of S_1, with the triangular elements so chosen that the shadow lines do not intersect any triangular element. The initial triangulation of S_1 is illustrated in Figure 3.3; a matching conforming triangulation is used for S_5 (for the 5-piece surface). The resulting triangulations $\mathcal{T}_n$ are referred to as a *discontinuity mesh*.

3.2. Test solutions. Among our test cases are the following true solutions u. In these cases, we calculate the emissivity E using highly accurate numerical integration. Then the collocation procedure is applied to find the approximate solution u_n, which is then compared to the known true solution. The accurate calculation of the collocation integrals of (2.43) is discussed in §4.

- We begin with a very well-behaved type of solution function.

$$u(x, y, z) = x^2 + y^2, \qquad (x, y, z) \in S. \tag{3.2}$$

  With this solution u, we can see the best type of behaviour that can be expected in our numerical procedures.
- The significance of the shadow lines in S_1 is that the first partial derivative of u is often discontinuous when the derivative is in a direction perpendicular to the shadow line. This affects the accuracy of the approximation $\mathcal{P}_n u \approx u$. To study this phenomena, we use the following true solution u:

(3.3)

$$u(x, y, z) = \begin{cases} \psi_\gamma(x, y) \left[(2B - x)_+ (2B - y)_+\right]^\beta, & (x, y, z) \in S_1, \\ 1, & (x, y, z) \in S_2 \cup S_3 \cup S_4, \\ 0, & (x, y, z) \in S_5, \end{cases}$$

$$\psi_\gamma(x, y) = e^{-\gamma(2B-x)(2B-y)}.$$

ETNA
Kent State University
etna@mcs.kent.edu

TABLE 3.1
Centroid method errors for u given by (3.2) and with a uniform mesh triangulation

4-Piece Surface			*5-Piece Surface*		
n	E_n	*Ratio*	n	E_n	*Ratio*
8	6.67		10	6.58	
32	0.910	7.3	40	3.28	2.01
128	0.214	4.3	160	1.86	1.76
512	0.0487	4.4	640	0.991	1.88
2048	0.0123	4.0	2560	0.511	1.94

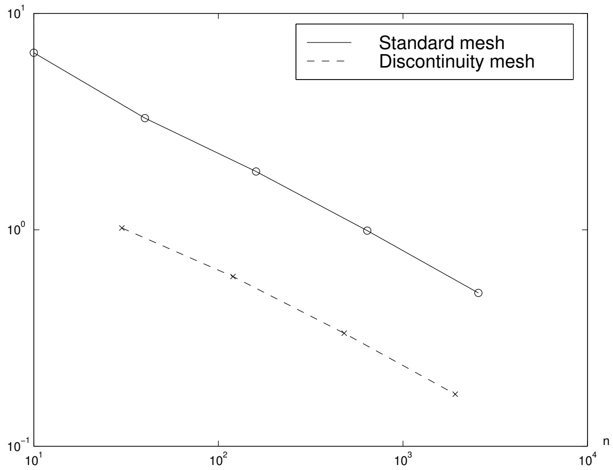

FIG. 3.4. *Errors with different meshing schemes, for centroid method and function (3.2) on 5-piece surface*

The function ψ_γ is used to decrease the size of $u(x, y, 0)$ away from the shadow line on the boundary of $[0, 2B] \times [0, 2B]$. The quantity $(f)_+$ is equal to f if $f \geq 0$, and it equals zero if $f < 0$. The exponent $\beta \geq 0$. With $\beta = 1$, we have a continuous non-linear function which has bounded, but some discontinuous first derivatives along the boundary of $[0, 2B] \times [0, 2B]$. With $\beta = \frac{1}{2}$, we have an algebraic singularity along this boundary, and we can study the effects of different types of triangulations for such a solution function. We choose $u \equiv 0$ on both S_5 (for the 5-piece surface) and on the subset of S_1 outside of the square $[0, 2B] \times [0, 2B]$.

- To study the ill-behaviour which can occur around at edge, we the numerical solution of the radiosity equation with the true solution

$$u(x,y,z) = \begin{cases} (A-y)^\beta, & (x,y,z) \in S_1, \\ 1, & (x,y,z) \in S_2 \cup S_3 \cup S_4, \\ 0, & (x,y,z) \in S_5. \end{cases} \tag{3.4}$$

In all cases, we use $\rho \equiv 1$. This does not present a problem, as we still have $\|\mathcal{K}\| < 1$ due to S not being a closed surface. We performed calculations with other choices of ρ, varying it over S. We have found that the case of $\rho \equiv 1$ is sufficient for illustrative purposes.

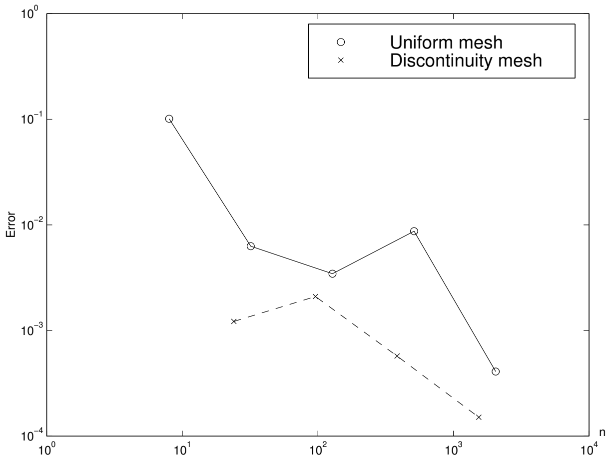

FIG. 3.5. *The centroid method errors (at the node points) for the u of (3.3) with $(\beta, \gamma) = (1.0, 1.5)$ on the 4-piece surface*

TABLE 3.2
Centroid method errors for u given by (3.3) with $(\beta, \gamma) = (0.5, 1.5)$

Uniform Mesh		*Discontinuity Mesh*		
n	E_n	n	E_n	*Ratio*
8	$7.97E-2$	24	$9.04E-4$	
32	$5.54E-3$	96	$1.50E-3$	
128	$5.65E-3$	384	$6.13E-4$	2.45
512	$5.22E-4$	1536	$2.31E-4$	2.65
2048	$1.38E-3$			

3.3. The centroid method. We first apply the centroid method for both the 4-piece and 5-piece surfaces. We begin with results for an ideally well-behaved u, that given by (3.2). The numerical results using the uniform mesh are given in Table 3.1; and the given error E_n is the maximum of the errors at the node points, as on the left side of (2.26). These numerical results are consistent with (2.26) and (2.30), showing a convergence of $O\left(h^2\right)$ for the 4-piece surface and approximately $O\left(h\right)$ for the 5-piece surface. The discontinuity meshing improved the error, but the results on the rate of convergence were quite similar. A comparison of the two forms of meshing is shown in Figure 3.4 for the 5-piece surface. The discontinuity meshing puts relatively more triangular elements into subsurface S_1 near to the edge at $y = A$; and this may account for the greater accuracy when solving the radiosity equation.

To see the effect of a discontinuity in a derivative of u along a shadow line, we solve for u given by (3.3) with $\beta = 1$ and $\gamma = 1.5$ for the 4-piece surface. We solve with both the uniform mesh and the discontinuity mesh. Graphs of these results are given in Figure 3.5; and the error with the discontinuity meshing is consistent with a convergence rate of $O\left(h^2\right)$. With the uniform meshing, the error is also consistent with $O\left(h^2\right)$ when the error for the coarsest mesh is compared to that of the finest mesh which we used. The discontinuity meshing is superior, both in accuracy and in the regularity of the behaviour of the error.

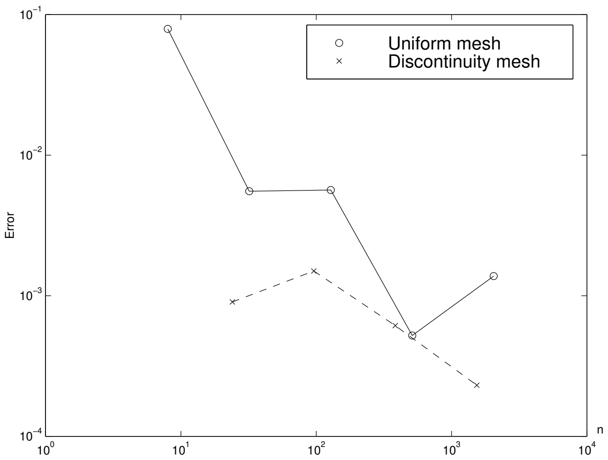

FIG. 3.6. *The centroid method errors (at the node points) for the uof (3.3) with* $(\beta, \gamma) = (0.5, 1.5)$.

TABLE 3.3
Centroid method errors for u *given by (3.4) with* $\beta = 0.5$ *on the 5-piece surface*

Uniform Mesh			*Discontinuity Mesh*		
n	E_n	*Ratio*	n	E_n	*Ratio*
10	.286		30	.0749	
40	.174	1.64	120	.0255	2.94
160	.124	1.40	480	.0177	1.44
640	.0879	1.41	1920	.0125	1.42
2560	.0622	1.41			

To see the effect of an algebraic singularity along the shadow line on the boundary of $[0, 2B] \times [0, 2B]$, we look at the case of u given by (3.3) with $\beta = 0.5$ and $\gamma = 1.5$ for the 4-piece surface. We solve with both the uniform mesh and the discontinuity mesh. Graphs of these results are given in Figure 3.6, and Table 3.2 contains the errors. Ratios are given only for the discontinuity meshing, as the convergence is so irregular for the uniform meshing. The final ratio given in the table is equivalent to a convergence rate of $O\left(h^{1.41}\right)$; and we expect it to improve to $O\left(h^{1.5}\right)$ as h decreases further, in line with (2.38). As with the previous case in Figure 3.5, using the uniform meshing gives a decrease in the error that is also consistent with $O\left(h^{1.5}\right)$, based on comparing the error for the coarse mesh to that of the finest mesh which we used. Still, the discontinuity meshing is superior, both in accuracy and in the regularity of the behaviour of the error.

To see the effect of an algebraic singularity along an edge, we consider the function u defined by (3.4) over the 5-piece surface, with $\beta = \frac{1}{2}$. We use both a uniform meshing and a discontinuity meshing, giving the results in Table 3.3. The results are consistent with a rate of convergence of $O(h^{.5})$, as is asserted in (2.30). As in the example of Figure 3.4, the error is smaller with the discontinuity meshing; and it is probably due to the mesh being relatively smaller near to $y = A$, the location of the singular behaviour in the solution u.

ETNA
Kent State University
etna@mcs.kent.edu

TABLE 3.4
Piecewise linear collocation method errors for u given by (3.2) with a uniform triangulation mesh

4-Piece Surface			*5-Piece Surface*		
n	E_n	*Ratio*	n	E_n	*Ratio*
8	1.43		10	1.44	
32	$2.13E-1$	6.71	40	$3.17E-1$	4.54
128	$8.89E-3$	24.0	160	$7.96E-2$	3.98
512	$2.74E-4$	32.5	640	$1.99E-2$	4.00

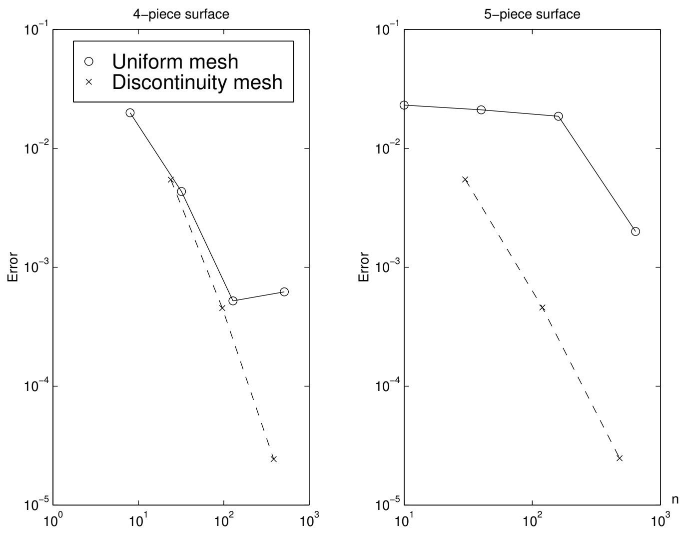

FIG. 3.7. *The piecewise linear collocation method errors (at the node points) for the u of (3.3) with* $(\beta, \gamma) = (1.0, 1.5)$

3.4. Piecewise linear collocation. We repeat the example of Table 3.1, with the unknown u of (3.2) and with both the 4-piece and 5-piece surfaces; and these results both use a uniform triangulation. The collocation nodes are defined using $\alpha = \frac{1}{6}$. These results are given in Table 3.4; note that the number of node points is $3n$. The results for the 4-piece surface illustrate and exceed the prediction of (2.42); and the results for the 5-piece surface illustrate (2.41).

To compare the use of uniform vs. discontinuity meshing, we again consider the u given by (3.3) for both the 4-piece and 5-piece surfaces, with $\beta = 1$ and $\gamma = 1.5$, and we use $\alpha = \frac{1}{6}$. The results are illustrated in Figure 3.7. For the 4-piece surface, the convergence results with discontinuity meshing are fairly consistent with the $O\left(h^4\right)$ predicted by (2.42) for the error at the node points, and there is an overall rate at all points of $O\left(h^2\right)$. For $n = 384$, the maximum error at the node points is 2.44×10^{-5}. With the uniform meshing, the results are more erratic, much as for the centroid method in this case. From the discussion in Subsection 2.5, the convergence will also be slower than with the discontinuity meshing, with at best $O\left(h^2\right)$ at the node points and $O\left(h\right)$ overall. The results for the 5-piece surface in this example are quite similar to those for the 4-piece surface when discontinuity meshing is used; and the results are worse in the case of the uniform spacing. Clearly, discontinuity

ETNA
Kent State University
etna@mcs.kent.edu

TABLE 3.5
Piecewise linear collocation method errors for u given by (3.4) with $\beta = 0.5$ and using a uniform triangulation mesh

4-Piece Surface			*5-Piece Surface*		
n	E_n	*Ratio*	n	E_n	*Ratio*
8	$1.98E-2$		10	$8.90E-2$	
32	$1.43E-3$	1.38	40	$6.32E-2$	1.41
128	$9.24E-5$	15.5	160	$4.46E-2$	1.42
512	$3.93E-5$	2.35	640	$3.16E-2$	1.41

meshing is important when dealing with 'shadow lines'.

We conclude by considering the solution u of (3.3) with $\beta = \frac{1}{2}$ and $\alpha = \frac{1}{6}$. The results for uniform meshing with both the 4-piece and 5-piece surfaces are given in Table 3.5. From the extension of the discussion following (2.38) to piecewise linear collocation, the order of convergence for the 4-piece surface should be $O\left(h^{1.5}\right)$; and the extension of (2.32) to piecewise linear collocation should yield a convergence of $O\left(h^{0.5}\right)$. The results in the table are consistent with what is expected for the 5-piece surface; whereas the ratios for the 4-piece surface would be expected to approach 2.83 as n increases, and they have not yet settled down to this in the table.

4. Calculation of the Collocation Integrals. The setup of the collocation linear system (2.43) requires the evaluation, potentially, of d_n^2 double integrals,

$$I_{i,j,\ell} = \int_{\Delta_j} V(P_i, Q) G(P_i, Q) \varphi_{k_{j,\ell}}(Q)\, dS_Q, \tag{4.1}$$

with $d_n = n$ and $3n$ for the centroid and piecewise linear methods, respectively. In fact, any scheme for setting up this linear system should recognize two factors which can decrease dramatically the number of such integrals needing to be evaluated. First, if P_i is located on the same subsurface of S as the triangular element Δ_j, then $G(P_i, Q) \equiv 0$ and thus the integral is zero. Second, if P_i cannot see any part of Δ_j, then $V(P_i, Q) \equiv 0$ over Δ_j and the integral is again zero. We consider now the evaluation of the remaining integrals (4.1).

We note one other point. If P_i can see only a portion of Δ_j, then the numerical scheme needs to know fairly precisely that portion. It is important to evaluate accurately the integrals over such partially visible elements. Doing otherwise will introduce new errors, and many schemes used in the past seriously degrade the accuracy attainable by the collocation method. Numerical examples show this quite clearly, although we omit such examples here.

Our initial schemes were based on first converting the integral in (4.1) to an integral

$$\int_\sigma g(s,t)\, d\sigma$$

over the unit simplex $\sigma = \{(s,t) : 0 \le s, t, s+t \le 1\}$. There are a number of numerical approximations to such integrals; cf. Stroud [22]. In particular, we have used the 3-point scheme

$$\int_\sigma g(s,t)\, d\sigma \approx \frac{1}{6}\left[g(q_1) + g(q_2) + g(q_3)\right], \tag{4.2}$$

with $\{q_i\}$ the midpoints of the sides of σ; and we have used the 7-point scheme

$$\int_\sigma g(s,t)\, d\sigma \approx \sum_{j=1}^{7} w_j g(\rho_j), \tag{4.3}$$

with the weights and nodes taken from the formula T2:5-1 of Stroud [22, p. 314]. The first of these has degree of precision 2 and the second has degree of precision 5. We used these to form composite numerical integration schemes over σ.

Subsequently, we used another well-known approach. Introduce the change of variables

$$s = (1-y)x, \qquad t = yx, \qquad 0 \le x, y \le 1.$$

With this, we have

$$\int_\sigma g(s,t)\, d\sigma = \int_0^1 \int_0^1 x\, g((1-y)x, yx)\, dx\, dy. \tag{4.4}$$

Apply Gauss-Legendre quadrature over the interval $[0,1]$ for both integrals. Originally, this scheme was intended to treat integrals in which g had some kind singular behaviour around $(s,t) = (0,0)$. Our numerical experiments have shown this scheme to generally be preferable (but not always) to composite schemes based on (4.2) or (4.3), even for smooth integrands g. For additional information on this approach to quadrature over σ, see [19]. An additional analysis of variable order composite quadrature schemes for integrals over σ is given in [18], although the focus is on singular and near-singular integrals.

Most of the integrals (4.1) are well-behaved and not difficult to evaluate. However, suppose P_i is located on a subsurface $\widetilde{S}$ of S, and suppose Δ_j is located on a subsurface $\widehat{S}$, with $\widetilde{S}$ and $\widehat{S}$ having a common edge. Then the integrand $G(P_i, Q)$ becomes increasingly ill-behaved as the distance between P_i and Δ_j decreases. To illustrate this, we consider the following special case.

Let $P = (x, 0, z)$ and $Q = (\xi, \eta, 0)$. We will consider the integrand $G(P,Q)$ over the region $\widehat{S} = [0,h] \times [0,h]$. Let $P = \left(\frac{1}{3}h, 0, \frac{1}{3}h\right)$, corresponding to P being the centroid of the triangle with vertices $(0,0,0)\,, (h,0,0)\,, (0,0,h)$. Then

$$G(P,Q) = \frac{\eta z}{\left[(x-\xi)^2 + \eta^2 + z^2\right]^2}.$$

To further simplify, let $(x, z, \xi, \eta) = h \cdot \left(\overline{x}, \overline{z}, \overline{\xi}, \overline{\eta}\right)$, with $\overline{x}, \overline{z}, \overline{\xi}, \overline{\eta}$ varying over $[0,1]$. Then

$$G(P,Q) = \frac{1}{h^2} \frac{\overline{\eta}\overline{z}}{\left[\left(\overline{x} - \overline{\xi}\right)^2 + \overline{\eta}^2 + \overline{z}^2\right]^2}.$$

This is unbounded over $\widehat{S}$ as $z, \eta \to 0$, assuming $x \in [0,h]$. Thus the integrand is increasingly peaked as $h \to 0$, with the domain $h\sigma$ becoming smaller.

Figure 4.1 contains a graph of G for an actual case using the 5-piece surface of §3, for piecewise linear collocation. The region of integration is the triangular domain bounded by the line segments joining the three points $(4.375, 5, 0)$, $(5, 4.375)$, and $(5, 5, 0)$ in the $\xi\eta$-plane; and $P \doteq (4.7917, 5.0, 0.0208)$. The maximum value of G over this region is approximately 750. This particular triangle is obtained in the uniform division of S_1 into 128 elements.

4.1. Analytic evaluation. It is important to be able to evaluate the integrals (4.1) accurately and efficiently. We have devised a method for analytic evaluation in the case of the collocation integrals for the centroid method, and an associated 'nearly-analytic' method for collocation of higher degree piecewise polynomial approximations, including piecewise linear collocation. The method is quite efficient, especially for nearly singular integrands such

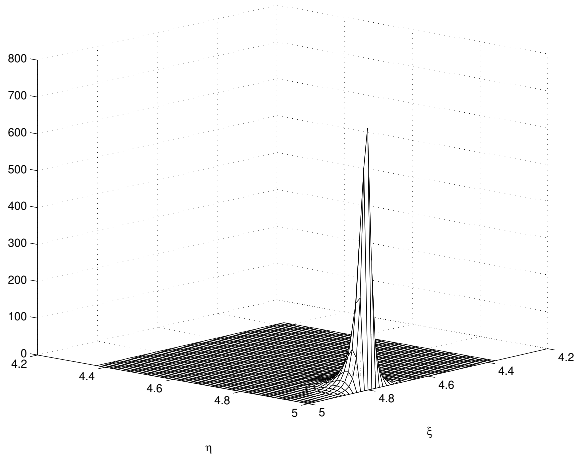

FIG. 4.1. *The function $G(P_i, Q)$ over a region in S_1 in the 5-piece surface with $P_i \in S_5$*

as that illustrated in Figure 4.1. It extends ideas of [14], developed for boundary integral equations, to the radiosity equation. In the cited case, all collocation integrals over polyhedral surfaces could be evaluated analytically. In contrast, we can only evaluate some of those integrals analytically; but all such integrals can be reduced to a much simpler form as one-variable integrals.

In this section, we describe the method we use to evaluate the integrals in (4.1). We assume every triangle Δ_j in (4.1) is a right triangle with vertices $\{v_1, v_2, v_3\}$. Since any triangle without a right angle can be divided into two right triangles, this assumption is not restrictive. Furthermore, v_1 is to be the vertex at the right angle and the other vertices are numbered counter-clockwise with respect to the inner normal vector given for the triangle. We begin by using an affine transformation to convert the integral in (4.1) to an integral

$$\int_{\sigma_{ab}} g(\xi, \eta)\, d\sigma$$

over the simplex

$$\sigma_{ab} = \left\{ (\xi, \eta, 0) : 0 \le \frac{\xi}{a}, \frac{\eta}{b}, \frac{\xi}{a} + \frac{\eta}{b} \le 1 \right\},$$

where a and b are the lengths of $\overline{v_1 v_2}$ and $\overline{v_1 v_3}$, respectively.

Let $P = (x, y, z)$ and $\mathbf{n}_p = (i, j, k)$, where $z > 0$ and $i^2 + j^2 + k^2 = 1$. Since σ_{ab} is in the xy-plane, we have $Q = (\xi, \eta, \zeta) = (\xi, \eta, 0)$ and $\mathbf{n}_q = (0, 0, 1)$. The integrals in

ETNA
Kent State University
etna@mcs.kent.edu

(4.1) are converted and simplified to the form of

$$
\begin{aligned}
&\int_{\sigma_{ab}} G(P,Q)\varphi(Q)\,d\sigma \\
&= \int_{\sigma_{ab}} \frac{((\xi-x)i+(\eta-y)j-zk)z(c_0+c_1\xi+c_2\eta)}{\left((x-\xi)^2+(y-\eta)^2+z^2\right)^2}\,d\sigma \\
&= \int_{\sigma_{ab}} \frac{zc_0((\xi-x)i+(\eta-y)j)}{\left((x-\xi)^2+(y-\eta)^2+z^2\right)^2}\,d\sigma && (4.5)\\
&+ \int_{\sigma_{ab}} \frac{((\xi-x)ic_2\eta+(\eta-y)jc_1\xi)z}{\left((x-\xi)^2+(y-\eta)^2+z^2\right)^2}\,d\sigma && (4.6)\\
&- \int_{\sigma_{ab}} \frac{z^2kc_0}{\left((x-\xi)^2+(y-\eta)^2+z^2\right)^2}\,d\sigma && (4.7)\\
&- \int_{\sigma_{ab}} \frac{z^2k(c_1\xi+c_2\eta)}{\left((x-\xi)^2+(y-\eta)^2+z^2\right)^2}\,d\sigma && (4.8)\\
&+ \int_{\sigma_{ab}} \frac{((\xi-x)ic_1\xi+(\eta-y)jc_2\eta)z}{\left((x-\xi)^2+(y-\eta)^2+z^2\right)^2}\,d\sigma, && (4.9)
\end{aligned}
$$

where the $c_i's$ are constants.

The integrals in (4.5) and (4.6) can be evaluated analytically and we give two examples here.

$$
\begin{aligned}
&\int_0^a \int_0^{b-\frac{b}{a}\xi} \frac{z\cdot(\eta-y)}{\left((\xi-x)^2+(\eta-y)^2+z^2\right)^2}\,d\eta d\xi \\
&= \frac{-az}{2\sqrt{(ab-ay-bx)^2+z^2(a^2+b^2)}}\left[\tan^{-1}\left(\frac{a^2+by-ax}{\sqrt{(ab-ay-bx)^2+z^2(a^2+b^2)}}\right)\right.\\
&\qquad\left.+\tan^{-1}\left(\frac{b^2-by+ax}{\sqrt{(ab-ay-bx)^2+z^2(a^2+b^2)}}\right)\right]\\
&+\frac{z}{2\sqrt{y^2+z^2}}\left[\tan^{-1}\left(\frac{a-x}{\sqrt{y^2+z^2}}\right)+\tan^{-1}\left(\frac{x}{\sqrt{y^2+z^2}}\right)\right].
\end{aligned}
$$

$$
\begin{aligned}
&\int_0^a \int_0^{b-\frac{b}{a}\xi} \frac{\xi\cdot z\cdot(\eta-y)}{\left((\xi-x)^2+(\eta-y)^2+z^2\right)^2}\,d\eta d\xi \\
&= \frac{z}{4}\left[\ln\frac{(a-x)^2+y^2+z^2}{x^2+y^2+z^2}-\frac{2x}{\sqrt{y^2+z^2}}\left(\tan^{-1}\left(\frac{x-a}{\sqrt{y^2+z^2}}\right)-\tan^{-1}\left(\frac{x}{\sqrt{y^2+z^2}}\right)\right)\right]\\
&-\frac{a^2z(b^2-by+ax)}{2(a^2+b^2)\sqrt{\%1}}\left[\tan^{-1}\left(\frac{b^2-by+ax}{\sqrt{\%1}}\right)+\tan^{-1}\left(\frac{a^2+by-ax}{\sqrt{\%1}}\right)\right]\\
&-\frac{a^2z}{4(a^2+b^2)}\left[\ln\left((a-x)^2+y^2+z^2\right)-\ln\left(x^2+(b-y)^2+z^2\right)\right],
\end{aligned}
$$

where $\%1 = a^2(b-y)^2+b^2(x^2+z^2-2ax)+a^2z^2+2abxy$.

ETNA
Kent State University
etna@mcs.kent.edu

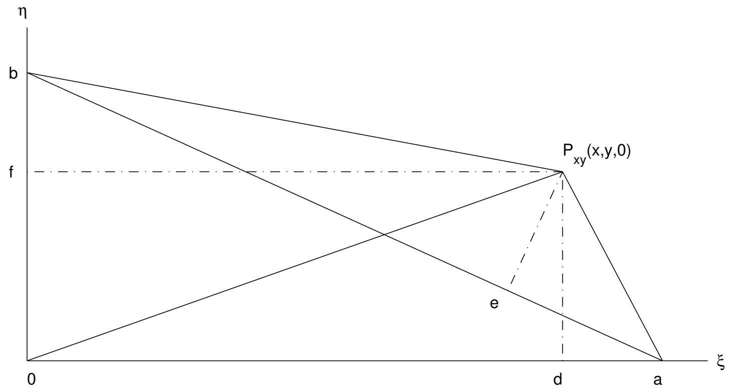

FIG. 4.2. *The decomposition of a general triangle associated with (4.11)*

The integral in (4.7) can not be analytically evaluated for an arbitrary point P in $\mathbb{R}^3$, but it can be evaluated for a special point. Let $P = (a,\, 0,\, z)$, $z > 0$, then

$$\begin{aligned} &\int_0^a \int_0^{b-\frac{b}{a}\xi} \frac{z^2 d\eta d\xi}{\left((x-\xi)^2 + (y-\eta)^2 + z^2\right)^2} \\ &= \int_0^a \int_0^{b-\frac{b}{a}\xi} \frac{z^2 d\eta d\xi}{\left((a-\xi)^2 + \eta^2 + z^2\right)^2} = \frac{az^2}{2\sqrt{a^2+z^2}} \tan^{-1}\left(\frac{b}{\sqrt{a^2+z^2}}\right). \end{aligned} \tag{4.10}$$

For an arbitrary point $P = (x,\, y,\, z)$, we apply the formula (4.10) six times. The geometry of the situation is shown in the Figure 4.2, where $P_{xy} = (x,\, y,\, 0)$ is the projection of the point P onto the xy-plane. The case shown is where P lies outside the triangle σ_{ab}. The integral over σ_{ab} becomes the sum of the integrals over the six triangles:

$$\int_{\sigma_{ab}} = \int_{\sigma_{dpo}} + \int_{\sigma_{dpa}} - \int_{\sigma_{epa}} - \int_{\sigma_{epb}} + \int_{\sigma_{fpb}} + \int_{\sigma_{fpo}}. \tag{4.11}$$

The integrals in (4.8) are the combinations of integrals in (4.5) and (4.7). For example,

$$\begin{aligned} &\int_{\sigma_{ab}} \frac{\xi}{\left((x-\xi)^2 + (y-\eta)^2 + z^2\right)^2}\, d\sigma \\ &= \int_{\sigma_{ab}} \frac{\xi - x}{\left((x-\xi)^2 + (y-\eta)^2 + z^2\right)^2}\, d\sigma + \int_{\sigma_{ab}} \frac{x}{\left((x-\xi)^2 + (y-\eta)^2 + z^2\right)^2}\, d\sigma. \end{aligned} \tag{4.12}$$

The first integral in (4.12) is the same type as (4.5) and the second integral is the same type as (4.7).

The integrals in (4.9) can be reduced to a one-dimensional integration, and it is evaluated with a numerical method. For example,

$$\int_0^a \int_0^{b-\frac{b}{a}\xi} \frac{\eta \cdot z \cdot (\eta - y)}{((\xi-x)^2+(\eta-y)^2+z^2)^2}\, d\eta d\xi$$
$$= \frac{1}{2}\int_0^a \int_0^{b-\frac{b}{a}\xi} \frac{z\, d\eta d\xi}{(\xi-x)^2+(\eta-y)^2+z^2} + \frac{abz}{4(a^2+b^2)}\left[\ln\frac{(a-x)^2+y^2+z^2}{x^2+(b-y)^2+z^2}\right]$$
$$- \frac{abz(a^2-ax+by)}{2(a^2+b^2)\sqrt{\%1}}\left[\tan^{-1}\left(\frac{a^2-ax+by}{\sqrt{\%1}}\right)+\tan^{-1}\left(\frac{b^2+ax-by}{\sqrt{\%1}}\right)\right].$$

This integral can not be evaluated analytically, but it is reduced to a one-dimensional integration.

$$\int_0^a \int_0^{b-\frac{b}{a}\xi} \frac{d\eta d\xi}{(\xi-x)^2+(\eta-y)^2+z^2}$$
$$= \int_0^a \frac{\tan^{-1}\left(\frac{\frac{b}{a}(x-\xi)-(y+\frac{bx}{a}-b)}{\sqrt{(\xi-x)^2+z^2}}\right)}{\sqrt{(\xi-x)^2+z^2}}\, d\xi + \int_0^a \frac{\tan^{-1}\left(\frac{y}{\sqrt{(\xi-x)^2+z^2}}\right)}{\sqrt{(\xi-x)^2+z^2}}\, d\xi. \tag{4.13}$$

In order to choose a better numerical integration scheme for (4.13), we simplify the integrals in it and then study the integrands of those simplified integrals. For the simplified integral, we let $(x, y, z) = (a, 0, z)$; and then following a simple change of variables, we have

$$\int_0^a \frac{\tan^{-1}\left(\frac{\frac{b}{a}(x-\xi)-(y+\frac{bx}{a}-b)}{\sqrt{(\xi-x)^2+z^2}}\right)}{\sqrt{(\xi-x)^2+z^2}}\, d\xi = \int_0^{\frac{a}{z}} \frac{\tan^{-1}\left(\frac{\frac{b}{a}u}{\sqrt{1+u^2}}\right)}{\sqrt{1+u^2}}\, du. \tag{4.14}$$

From the Figure 4.3 for the right-hand integrand, we can see that the integrand increases very rapidly around zero, and it stays relatively flat around one and beyond. Also, it goes up faster as the number b/a gets larger. For the integrand with such behaviour, we use the IMT numerical integration method [2, p. 307]. We use it with 128 nodes, which appears to be more than is needed for the cases we have dealt with.

The integrals (4.5)–(4.9) are used for the case of approximating the solution u with linear functions. For the centroid method, which approximates the solution u with constant functions, only the integrals in (4.5) and (4.7) are used, and thus all needed integrals can be evaluated analytically.

4.2. Numerical examples. We present some timing and error comparisons on the various means of setting up the collocation matrix of (2.43). Before doing so, we review the three methods of evaluation. The first method was described directly above in §4.1, and we refer to it as the *exact method*. It uses analytic evaluation of the collocation integrals for the centroid method. For piecewise linear collocation, it uses a mix of analytic evaluation and numerical evaluation of some one-dimensional integrals, as described above following (4.14). Recall that for each call on the IMT quadrature method, we have chosen to use 128 nodes, to ensure sufficient accuracy.

The second method of evaluating the collocation integrals is a composite method based on the 7-point rule of (4.3), and we refer to it as the *7-point method*. The third method uses the change of variable given in (4.4), followed by Gaussian quadrature in each variable; we refer to this as the *Gauss method*. With the second method, we have a parameter *MaxLev* to determine the number of subdivisions to be used in the composite rule; and referring to the

ETNA
Kent State University
etna@mcs.kent.edu

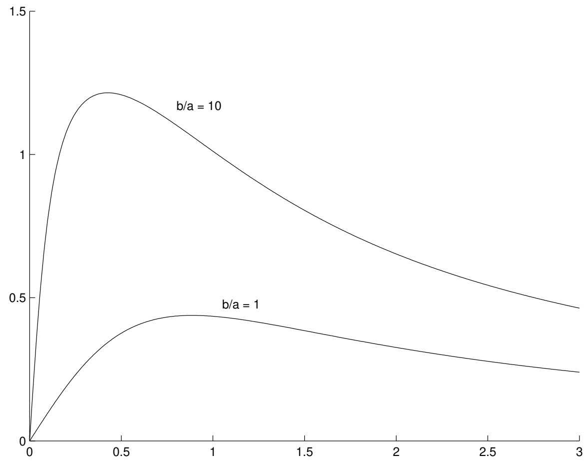

FIG. 4.3. *The integrand for single variable integration with varying b/a*

collocation integral in (4.1), the number of subdivisions also depends on the distance between the field point P_i and the integration region Δ_j. When this distance is small, we divide Δ_j into 4^{MaxLev} smaller congruent triangles, applying the 7-point rule over each of them. As the distance between P_i and Δ_j increases, we use a smaller exponent, gradually having it decrease to 0 (corresponding to applying the 7-point rule over the full triangle Δ_j). This is described in greater detail in both [3, p. 460] and [4].

The third method uses two parameters, *IBase* and *MaxLev*. As with the second method, we use the largest number of nodes when P_i and Δ_j are closest, decreasing the number of nodes as the distance between P_i and Δ_j increases. We begin by using Gauss-Legendre quadrature with $2^{IBase+MaxLev}$ nodes in each dimension of (4.4), decreasing it eventually to 2^{IBase} nodes.

For the numerical examples, we set up the linear system for solving the radiosity equation with $u = x^2 + y^2$ on S, as in (3.2). We then solved the linear system and looked at the error in the solution. We have chosen the parameters so as to have the quadrature error be small enough as to match the best possible for the given value of n, the number of triangular elements being used. The timings given below are for the setup time for the matrix in (2.43). For our values of n, this dominated all other times (except for calculating the emissivity function with the given true value of u). We give timings for only the 5-piece surface, as that involves the more practical situation in which two subsurfaces share a common edge.

Tables 4.1 and 4.2 contain the timings and errors (maximum at the node points) for the centroid collocation method and piecewise linear collocation method, respectively. The timings were done on a Hewlett-Packard C200 workstation with a 200MHz PA-8200 CPU, 768MB RAM. The machine was networked, but otherwise was restricted to only the given program being timed; and several runs were made, with the lowest timings given in the tables. For the centroid collocation method, the 7-point method used *MaxLev*=3, and the Gauss method used (*IBase,MaxLev*)=(1,3). For the piecewise linear collocation method, we used (*IBase,MaxLev*)=(1,4) and (1,5). The timings for the smaller values of n are unreliable, but are indicative of the magnitude of time being used. The errors may seem large, but note that the solution is also large; and thus an error of 0.511 corresponds to an approximate relative

TABLE 4.1
Centroid collocation errors for u given by (3.2), for varying integration methods

	$Exact$		$7-Point$		$Gauss$	
n	$Error$	$Time$	$Error$	$Time$	$Error$	$Time$
40	3.28	.031	3.28	4.11	3.28	.594
160	1.86	.469	1.86	32.7	1.85	4.93
640	.991	7.12	.991	163	.986	84.2
2560	.511	111	.510	846	.506	2940

TABLE 4.2
Piecewise linear collocation errors for u given by (3.2), for varying integration methods

	$Exact$		$Gauss : MaxLev = 4$		$Gauss : MaxLev = 5$	
n	$Error$	$Time$	$Error$	$Time$	$Error$	$Time$
10	1.44	.164	1.44	3.52	1.44	14.2
40	.317	1.79	.317	34.8	.317	139
160	.0796	29.3	.0795	158	.0796	625
640	.0199	474	.103	558	.0199	2150

error of 0.01. Also recall that with piecewise linear collocation, the order of the linear system (2.43) is $3n$.

It is clear by comparing the two tables for the *Exact* method that the integrals for the piecewise linear collocation are more costly to evaluate. This is due to both the more complicated form of the integration and to the use of the IMT method for the one-dimensional integration. It is also clear that the use of the *Exact* method is preferable over the *Gauss method* as regards running time. This will become even clearer for larger values of n, as then the parameters *MaxLev* and *IBase* will need to be increased, which will again increase significantly the cost of the quadratures. Also, with the greater accuracy possible with piecewise linear collocation, one also needs greater accuracy in calculating the coefficients. This is seen in Table 4.2 in comparing the *Gauss method* for the parameter values of *MaxLev*. Clearly, the higher value *MaxLev=5* is needed, but it is also quite expensive when compared to the *Exact method*. The same type of results are true for the 7-point method, and it is due to the type of singular behaviour illustrated in Figure 4.1. If numerical integration is to be used, it must be more carefully designed than the methods we have used here.

Acknowledgements. The authors would like to thank Dr. Olaf Hansen for a number of helpful suggestions and discussions.

REFERENCES

[1] K. ATKINSON, *Piecewise polynomial collocation for integral equations on surfaces in three dimensions*, J. Integral Equations, 9 (1985), suppl., pp. 25-48.

[2] K. ATKINSON, *An Introduction to Numerical Analysis*, Second edition, John Wiley & Sons, Inc., New York, 1989.

[3] K. ATKINSON, *The Numerical Solution of Integral Equations of the Second Kind*, Cambridge University Press, Cambridge, 1997.

[4] K. ATKINSON, *User's Guide to a Boundary Element Package for Solving Integral Equations on Piecewise Smooth Surfaces* (Release #2), Reports on Computational Mathematics #103, Dept of Mathematics, University of Iowa, Iowa City, 1998. The programs and guide are available via the URL http://www.math.uiowa.edu/~atkinson/bie.html.

[5] K. ATKINSON, *The planar radiosity equation and its numerical solution*, IMA J. Numer. Anal., 20 (2000), pp. 303-332.

[6] K. Atkinson and G. Chandler, *The collocation method for solving the radiosity equation for unoccluded surfaces*, J. Integral Equations Appl., 10 (1998), pp. 253-290.
[7] K. Atkinson and D. Chien, *A fast matrix-vector multiplication method for solving the radiosity equation*, Adv. Comput. Math., 12 (2000), pp. 151-174.
[8] K. Atkinson, I. Graham, and I. Sloan, *Piecewise continuous collocation for integral equations*, SIAM J. Numer. Anal., 20 (1983), pp. 172-186.
[9] G. Chandler and I. Graham, *Product integration-collocation methods for non-compact integral operator equations*, Math. Comp., 50 (1988), pp. 125-138.
[10] M. Cohen and J. Wallace, *Radiosity and Realistic Image Synthesis*, Academic Press Inc., New York, 1993.
[11] M. Costabel and E. Stephan, *Boundary integral equations for mixed boundary value problems in polygonal domains and Galerkin approximation*, in Mathematical Models and Methods in Mechanics, Banach Center Publications, Warsaw, 15 (1985), pp. 175-251.
[12] J. Elschner, *On spline approximation for a class of non-compact integral equations*, Math. Nachr., 146 (1990), pp. 271-321.
[13] S. Gortler, P. Schröder, M. Cohen, and P. Hanrahan, *Wavelet radiosity*, Comput. Graph. Proc., Annual conference series, 1993, pp. 221-230.
[14] F. Johnson, *A general panel method for the analysis and design of arbitrary configurations in incompressible flow*, NASA Tech. Rep. NASA-CR-3079, Nat. Tech. Inform. Service, Springfield, VA, 1980.
[15] D. Lischinski, F. Tampieri, and D. Greenberg, *Discontinuity meshing for accurate radiosity*, IEEE Comput. Graph. Appl., 12 (1992), pp. 25-39.
[16] A. Rathsfeld, *Edge asymptotics for the radiosity equation over polyhedral boundaries*, Math. Methods Appl. Sci., 22 (1999), pp. 217-241.
[17] Henning Schon, *Effiziente Verfahren zur numerischen Lösung der Radiosity-Gleichung*, PhD thesis, University of Karlsruhe, 1997.
[18] C. Schwab, *Variable order composite quadrature of singular and nearly singular integrals*, Computing, 53 (1994), pp. 173-194.
[19] C. Schwab and W. Wendland, *On numerical cubatures of singular surface integrals in boundary element methods*, Numer. Math., 62 (1992), pp. 343-369.
[20] J. Seol, *Solving the Occluded Radiosity Equation using Collocation Methods*, PhD thesis, anticipated 2001, Univ. of Iowa, Iowa City.
[21] F. Sillion and C. Puech, *Radiosity and Global Illumination*, Morgan Kaufmann Publishing Co., San Francisco, 1994.
[22] A. Stroud, *Approximate Calculation of Multiple Integrals*, Prentice-Hall Inc., Englewood Cliffs, New Jersey, 1971.